High-density covalent grafting of spin-active molecular moieties to diamond surfaces

Benjamin F. Bachman[†], Zachary R. Jones[†], Gabriel R. Jaffe[‡], Jad Salman[⊥], Raymond Wambold[⊥], Zhaoning Yu[‡,⊥], Jennifer T. Choy[§], Shimon J. Kolkowitz[‡], Mark A. Eriksson[‡], Mikhail A. Kats[‡,⊥], Robert J. Hamers[†]*

†Department of Chemistry, University of Wisconsin – Madison, 1101 University Avenue, Madison WI 53706

‡Department of Physics, University of Wisconsin – Madison, 1150 University Avenue, Madison WI 53706

⊥Department of Electrical and Computer Engineering, University of Wisconsin – Madison 1415 Engineering Drive, Madison, WI 53706

§Department of Engineering Physics, University of Wisconsin – Madison, 1500 Engineering Drive, Madison, WI 53706

*Corresponding Author

KEYWORDS: Diamond, Spin probe, TEMPO, nanoparticle, surfaces

ABSTRACT

Functionalization of diamond surfaces with TEMPO and other surface paramagnetic species represents one approach to implementation of novel chemical detection schemes that

make use of shallow quantum color defects such as silicon-vacancy (SiV) and nitrogen-vacancy (NV) centers. Yet, prior approaches to quantum-based chemical sensing have been hampered by the absence of high-quality surface functionalization schemes for linking radicals to diamond surfaces. Here, we demonstrate a highly controlled approach to functionalization of diamond surfaces with carboxylic acid groups via all-carbon tethers of different lengths, followed by covalent chemistry to yield high-quality, TEMPO-modified surfaces. Our studies yield estimated surface densities of 4-amino-TEMPO of approximately 1.4 molecules nm^{-2} on nanodiamond (varying with molecular linker length) and 3.3 molecules nm-^{2} on planar diamond. These values are higher than those reported previously using other functionalization methods. The ζ-potential of nanodiamonds was used to track reaction progress and elucidate the regioselectivity of the reaction between ethenyl- and carboxylate-groups with surface radicals.

INTRODUCTION

Diamond is renowned for its many outstanding physical and chemical properties[1-3] The highly stable surface chemistry of diamond and other carbon-based materials provides a robust platform for applications that involve harsh chemical environments.[4-6] Recent studies have demonstrated how surface chemistry of diamond can play an important role in emerging applications such as quantum information storage and new chemical imaging approaches that make use of the unique properties of near-surface quantum defects such as nitrogen-vacancy (NV) and silicon-vacancy (SiV) centers in diamond.[7-10]

One key challenge in diamond surface chemistry is that the high strength of C-C, C-O, and C-N bonds, typically necessitate the use of harsh conditions both to prepare the initial surface and to induce subsequent modifications. Carboxylate groups are among the most versatile functional groups in organic chemistry and are typically produced on diamond surfaces

by exposure to hot mineral acids.[11] However, these conditions etch and roughen the diamond surface and also produce a heterogeneous distribution of oxidized carbon functionalities.[12] An alternative approach to preparing carboxylic-acid-terminated diamond is to graft carboxylic-acid-bearing molecules to a suitably prepared hydrogen-terminated surface. Smooth, H-terminated diamond surfaces can be prepared using hydrogen plasmas or by heating in H_2 gas. [13-15] Liquid-phase terminal ethenyl-groups will graft to H-terminated diamond surfaces when excited by ultraviolet light (UV).[4, 16] However, harsh UV light can also induce polymerization reactions of reactants bearing conjugated bonds or other UV-active chromophores. [16-17] Recently, the use of radical initiators was demonstrated as an alternative, scalable way to initiate grafting of molecules with an ethenyl-group to diamond forming a robust all-carbon scaffold for further functionalization. [17] Previous work has shown that radical-induced grafting of simple alkanes bearing carboxylate groups formed surface ether linkages; our work shows that if the molecules also have an ethenyl group, grafting occurs through this group, leaving the carboxylate group exposed and accessible for subsequent manipulations.[18] While both UV and radical initiators can produce functionalized diamond surfaces, subsequent modification with complex, delicate molecules, such as those bearing unpaired electron spins of interest for spin-based chemical detection, has not been previously shown.[7-8]

Here, we demonstrate the ability to prepare diamond surfaces functionalized with aminoxyl radicals with control over the distance from the radical site to the diamond surface. Figure 1 shows a simplified step-by-step chemical route to functionalize diamond with 4-amino-TEMPO through amide bonds. We use the stable radical TEMPO as a model system due to its relatively high stability and widespread use as a model organic radical. Electron-spin resonance studies of TEMPO-modified diamond nanoparticles show that the grafted TEMPO molecules

retain their radical character as measured by electron paramagnetic resonance (EPR) when grafted to the surface. [7-8] EPR and X-ray photoelectron spectroscopy (XPS) data show that the surface-tethered TEMPO molecules are covalently linked to the surface and retain their radical character. The removal of sp^2-hybridized, "graphitic" carbon from the surface is important for increasing fluorescence intensity from near-surface defects as well as suppressing background fluorescence due to graphitic carbon for optical sensing.[19] This surface cleaning may be achieved through exposure to mixed mineral acids or though annealing in air.[20] Oxidation of nanodiamond surfaces has also shown to decrease the spin-noise of shallow quantum defects used for chemical sensing. [21] This work provides a pathway to preparation of surfaces with controlled electron spin densities that may be particularly impactful for emerging approaches to quantum sensing and quantum information storage.

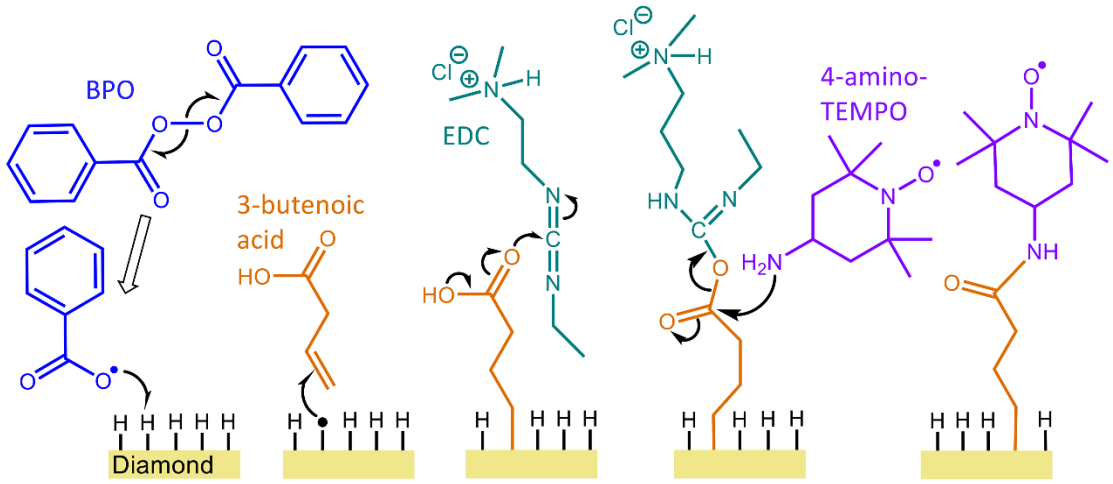

Figure 1: *Simplified multistep functionalization mechanism to graft carboxylic acid and 4-amino-TEMPO to diamond. Not shown is the impact of the sulfo-NHS catalyst.*

EXPERIMENTAL

2.1 Materials and Chemicals:

All nanodiamond experiments were carried out on monocrystalline nanodiamond from Microdiamant (MSY 0 – 0.25 μm, 125 nm average diameter). Single-crystal (111) high-pressure high-temperature (HPHT) planar diamond samples were obtained from Element 6 (145-500-0561). Chemicals used for carboxylate and TEMPO functionalizing diamond include: 2-propenoic acid (#147230), 3-butenoic acid (#134716), 4-pentenoic acid (#245925), 5-hexenoic acid (#464920), 8-nonenoic acid (#715433), 10-undecenoic acid (#124672), benzoyl peroxide (BPO) (#179981), anhydrous benzene (#401765), acetone (#179124), ethanol (#459844), N-Hydroxysulfosuccinimide sodium salt (Sulfo-NHS) (#56485), N-(3-Dimethylaminopropyl)-N'-ethylcarbodiimide hydrochloride (EDC) (#03449), 4-amino-TEMPO (#163945), 2-(N-Morpholino)ethanesulfonic (MES) acid monohydrate (#69892), potassium chloride (#P3911), and potassium bromide (#221864). No extra purification steps were taken to remove the radical inhibitors from the 2-propenoic acid (200 ppm MEHQ) and 3-butenoic acid solutions. All water used was obtained from a Barnstead NanoPure water system with resistivity >18.2 MΩ cm.

2.2 Removal of surface graphitic contaminants:

Surface sp^2-hydrized carbon was removed from nanodiamond by annealing in air at 590 °C for 2 hours after a 20-minute ramp in a tube furnace using an alumina boat following a modified version of the procedure published previously.[22] After only one hour, the color of the diamond lightened, but remained grey, indicating the presence of residual surface graphitic carbon. After two hours, the nanodiamond changed from grey to white, with a slight yellow coloration that we attribute to nitrogen impurities in the diamond.[23] After five hours, the remaining diamond was yellow, resembling that of Type Ib crystalline diamonds. Much of the diamond was lost to oxidation during the annealing, consistent with prior reports.[20, 23] We performed a gravimetric analysis of one batch annealed for 2 hours and found that 91.4 ± 0.3%

of the diamond was lost to combustion. Longer heating times resulted in unacceptably high loss and were not pursued.

2.3 H-termination of Diamond Samples:

To help understand the influence of air-annealing, we hydrogen-terminated both air-annealed nanodiamond and non-annealed (as-received) nanodiamond as described above. In both, H-termination was carried out in a tube furnace at 750 °C for 5 hours under a flow of 50 standard cubic centimeters per minute (sccm) ultra-high purity H_2 (Airgas #HY UHP300) at atmospheric pressure. H-termination of nanodiamond after air-annealing resulted in a further mass loss of 2.2 ± 0.3 %, while non-annealed nanodiamond lost 1.0 ± 0.3 %. The air-annealed nanoparticles developed a very light grey coloration after H-termination, suggesting the presence of a small amount of sp^2-carbon, yet these samples were much lighter in color than the H-terminated samples that were not previously air-annealed (see Fig. 1 in SI). The surface area of air-annealed nanodiamond (46.55 m^2/g) was determined by Brunauer-Emmett-Teller (BET) surface area analysis using a micrometrics Gemini VII version 2.00 instrument. We also performed experiments using planar monocrystalline diamond samples that were H-terminated in a modified AsTEX SDS 5010 microwave plasma chemical vapor deposition reactor (MPCVD). Ultra-high purity H_2 flowing at 200 sccm at a pressure of 3 Torr was used to ignite the plasma; the pressure was then increased to 48 Torr and power increased to 600 W for 15 minutes. Samples were then allowed to cool to room temperature under a constant flow of H_2.

2.4 Functionalization of diamond samples with carboxylate groups

H-terminated nanodiamond was added to a glass centrifuge tube and transferred into an argon glovebox. A small sample of this powder was removed for analysis by dynamic light-scattering (DLS). Anhydrous benzene was added to the remaining diamond, and 5 mL aliquots of

the benzene-nanodiamond slurry were then added to glass centrifuge tubes. An ethenyl-terminated carboxylic acid and benzoyl peroxide was then added to the diamond slurry to yield 100 mM concentrations in the final mixture. Benzoyl peroxide dissociates into two benzoate radicals at temperature above 79.8 °C in benzene.[24] Based on a BET surface area measurement, we estimate that the reactant liquid contains a 9-fold excess of benzoate initiator radicals compared to the total number of surface C atoms exposed on the nanodiamond.

Each glass centrifuge tube was sealed with a Teflon-coated stir-bar inside and then agitated using a water-cooled cup ultrasonicator (Cole-Parmer model CPX750) in continuous mode with a power of 21.5 W for 10 minutes. The tubes were then placed in an oil bath and heated to 80 °C for different amounts of time while stirring vigorously; this heating step activates the benzoyl peroxide radical initiator. The samples were then cooled to room temperature in air followed by ultrasonic agitation for 10 minutes at 21.5 W. Procedures for cleaning the functionalized samples to eliminate physisorbed material and other contaminants varied slightly with the reactant molecule used, due to differences in physical properties of the reactant mixtures; detailed procedures are described in the SI. While most experiments reported here were performed using nanodiamond, a limited number of experiments were performed using a single-crystal diamond (111) that was H-terminated by microwave plasma and then functionalized with 2-propenoic acid following the same procedure used with nanoparticles.[13] After grafting 2-propenoic acid, the planar diamond was ultrasonicated for 10 minutes in continuous mode with a power of 21.5 W, first in the reactant/benzene mixture followed by successive rinses in 5 mL solutions of neat acetone and water for a total of 30 minutes of sonication.

2.5 TEMPO-functionalization of carboxylate-modified diamond samples:

Each sample of functionalized nanodiamond was divided into two aliquots. To one aliquot, we added 40 mL of 20 mM MES , 6.3 mg EDC (yielding 0.8 mM EDC), and 8.63 mg sulfo-NHS (yielding 1 mM sulfo-NHS). The second aliquot was prepared identically except that no EDC was added; these samples are referred to as "no-EDC control" samples. We added 6.85 mg 4-amino-TEMPO ((yielding 1 mM) to each sample, which was then sealed and mounted to a rotisserie shaker (Barnstead Labquake #C415110) for 12 hours. The samples were ultrasonicated for 60 seconds at 21.5 W; samples that were functionalized with 8-nonanoic and 10-undecenoic acids received an additional 3 and 10 minutes of ultrasonication respectively to ensure removal of any visible aggregates. Samples were then centrifuged at 4700×*g* for at least 20 minutes until all samples form pellets. Samples originally functionalized with 10-undecenoic acid show significant adhesion to the walls of the samples tube, while 8-nonenoic acid samples showing less adhesion. All subsequent rinsing was done with 40 mL of solution, ultrasonication for 60 seconds each at 21.5 W and centrifugation for a minimum of 20 minutes. The first rinse was water, the 2nd and 3rd were with 100 mM KCl, and the 4th – 6th are with water again, for a total of 280 mL solution and a minimum of 6 minutes of ultrasonication.

The planar diamond sample with grafted carboxylate groups was TEMPO-functionalized following the same procedure as used with nanodiamond up to the rinsing step. After TEMPO functionalization, the sample was ultrasonicated for 60 seconds at 30 % power in the TEMPO solution, followed by a 15 mL solutions of 100 mM KCl, and then water, for a total of 3 minutes of sonication.

2.6 Dynamic light-scattering ζ-potential measurements:

Dynamic light-scattering (DLS) and ζ-potential measurements were taken on a Malvern Zetasizer instrument using 1 mL folded capillary cells (DTS1060). DLS samples were taken at a

concentration of ~$4x10^8$ nanoparticles/mL and were prepared from samples of functionalized nanoparticle after the final rinsing step of each procedure. The as-received, air-annealed, and H-terminated, nanodiamond samples were introduced into pure water and sonicated for 60 seconds at 21.5 W to suspend. Both size and ζ-potential (ZP) measurements are taken 5 times with 10 runs each at room temperature. DLS measurements are taken before ZP measurement. The conductivity and average count rate of the acid-terminated, no-EDC control, and TEMPO-functionalized samples, was 0.011±0.003 mS/cm and 59,000±11,000 kilo counts per second respectively, and all the same within error. Refractive index values of 2.40 for the nanoparticles and 1.330 for the dispersant we used. Because previous studies have shown that ultrasonication of nanodiamond can induced changes in ZP (likely due to mechanical damage), we did not perform ultrasonication on the nanodiamond samples shown in Figs. 2 or 5. [25]

2.7 XPS measurements:

XPS measurements were taken with a Thermo Kα instrument with an Al K_α source, a 400 μm spot size, capturing electrons emitted at 45° with respect to the surface normal, and using an electron flood gun to reduce charging effects. We used a pass energy of 50 eV with a 0.2 eV step size. Samples of TEMPO-functionalized nanoparticles were collected from the pellet formed after the final centrifugation step of each washing process, but before the addition of water and ultrasonication. All nanodiamond samples were drop-cast from water onto Si wafer chips. Planar diamond samples were used after all rinsing steps detailed above. All XPS spectra were analyzed using CasaXPS software. [26] Peak positions were corrected by normalizing all peaks to the adventitious carbon sp^2 peak at 284.7 eV.[27] TEMPO surface coverages were estimated by integrating the N(1s) and C(1s) peaks and using the C(1s) intensity as an internal standard.

2.8 EPR measurements:

EPR measurements were collected with an X-band continuous-wave Bruker ELEXSYS E500 EPR Spectrometer equipped with a SuperX high-power microwave bridge and a Super Hi-Q resonator. EPR samples were prepared by drop-casting pelleted nanodiamond slurry into 4 mm Wilmad quartz EPR tubes from Sigma (#Z567361). The EPR tubes were then sealed inside 15 mL centrifuge tubes and centrifuged at 3005×g for 10 minutes to pellet the diamond at the bottom of the tube. *Safety Note: We note that EPR tubes sometimes shattered inside the centrifuge tube when run at the higher centrifugal force (4700×g) used elsewhere in this work; use extreme caution in this step.* EPR samples were then dried overnight in a vacuum oven at 30 ^{o}C. A 4 μL aliquot of water was added to each sample before EPR analysis. We added an additional step of centrifuging the wet EPR samples in a manual centrifuge (Hettich Handzentrifuge centrifuge) to ensure all the water was at the bottom of the quartz sample tube with the nanodiamond. All EPR spectra were measured with a modulation amplitude of 1 G and a microwave power of 50.24 μW. To make the diamond calibration standards, freshly annealed and H-terminated nanodiamond of known mass was added to an EPR tube and hand-centrifuged to concentrate at the bottom of the tube. A TEMPO calibration curve was made by integrating the total EPR signal from five different aliquots (4 μL each) aqueous solutions of 4-amino-TEMPO to a simple linear regression with an R^2 of 0.988. EPR spectra were integrated, and a linear baseline correction was applied using the IGOR program.

2.9 DRIFTS measurements:

Diffuse-reflectance infrared Fourier-transform spectroscopy (DRIFTS) measurements of nanodiamond samples are collected with a Vertex 70v FT-IR spectrometer with a Harrick

Praying Mantis accessory. Nanodiamond particles are diluted to 5% by mass in KBr in an inert-atmosphere glovebox before sample loading into N_2-purged atmosphere for data collection.

RESULTS

3.1 DLS and ζ-potential analysis of functionalized nanodiamond.

We conducted DLS and ζ-potential experiments on H-terminated air-annealed nanodiamond to determine grafting rates. Fig. 2 shows the ZP of nanodiamond samples after grafting with 10-undecenoic acid for different lengths of time, starting with air-annealed diamond samples that were then H-terminated as described above. Fig. 2 shows that H-terminated nanodiamond samples initially have a positive ZP, consistent with prior studies.[28-29] As the grafting reaction proceeds, the ZP becomes more negative due to the surface carboxylate groups, also in agreement with prior studies. [29] Our data suggest that the initial grafting of reactant molecules is complete within approximately 30 minutes. ZP analysis of air-annealed diamond functionalized for 24 hours by various ethenyl-bearing carboxylic acids with carbon-carbon chain lengths between 2 and 10 showed an average ZP of -39±3 mV.

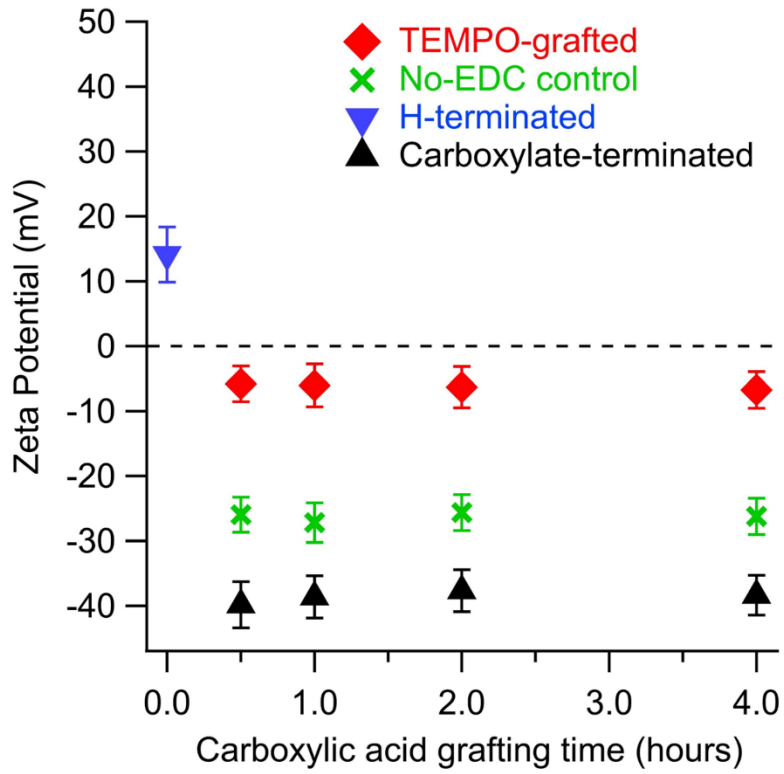

Figure 2: *Variation in zeta-potential of H-terminated nanodiamond with a prior air-anneal as a function of the duration of initial grafting of 10-undecenoic acid. Carboxylate-functionalized samples were then exposed to an aqueous solution of 4-amino-TEMPO with and without the EDC crosslinker.*

While the data in Fig. 2 suggests that 30-minutes is the longest reaction time necessary, all samples used in this work were grafted for 24 hours to ensure that surface reactions to come to completion. The second reaction step, coupling of 4-amino-TEMPO to the carboxylate-terminated surfaces, was then performed. Fig. 2 shows how the ZP of the resulting samples depends on the exposed surface functional groups, along with the results of control experiments in which the EDC cross-linker was intentionally left out. A comparison of the sample with and without EDC shows that including EDC in the reactant mixture greatly shifts the ZP to more positive values, consistent with the role of EDC in facilitating coupling of TEMPO to the

surface. The “No-EDC” control sample shows a slight shift to positive potential compared with the carboxylate-functionalized surface. This shift likely arises from a small amount of residual physiosorbed TEMPO. Our data suggests that the H-terminated nanodiamond was successfully functionalized with carboxylate groups and subsequently covalently linked to 4-amino-TEMPO.

3.2 XPS analysis of functionalized diamond

We quantified the coverage of grafted carboxylate groups and subsequently functionalized 4-amino-TEMPO molecules using XPS analysis. Fig. 3A shows C(1s) spectra of a high-temperature high-pressure (HTHP) planar diamond (111) sample after surface termination with carboxylate groups and again after the subsequent steps to functionalize with TEMPO. The C(1s) spectrum after grafting of 2-propenoic acid exhibits two clear peaks at 289.8 and 284.8 eV. The peak at the higher (289.8 eV) binding energy, which we attribute to C atoms in carboxylate groups, accounts for 3.8 % of the total C(1s) area. The energy and fractional area of this peak are comparable to prior literature values (4.7 %) on single-crystal diamond (111) samples after exposure to using hot mineral acids.[11]. Fig. 3A also shows a change in peak shape upon TEMPO functionalization, with a decrease in intensity near 289.4 eV and an increase near 287 eV, a range typically attributed to carbon in C-O-C and C-O-H moieties. [30] Fig. 3B shows the N(1s) peak of both nano- and planar-diamond samples grafted with 2-propenoic acid and functionalized with 4-amino-TEMPO both with and without EDC; all three spectra are presented on the same vertical scale, but due to differences in number spectra averaged together the signal-to-noise ratio differs between nanodiamond and planar samples samples. XPS analysis of no-EDC control samples show no detectable N(1s) signal. We estimated our detection limit based on the observed peak height and the signal-to-noise of the functionalized planar diamond and a control measured under identical conditions. Based on this analysis we determined that a N

coverage of 0.25 N atoms nm^{-2} would yield a peak with height twice the standard deviation of the data under the conditions of our experiment. We therefore conclude that our N coverage is less than 0.25 atoms nm^{-2} . The absence of detectable N from the no-EDC control samples indicates that 4-amino-TEMPO linked to the diamond with the assistance of EDC is covalently linked through stable amide bonds.

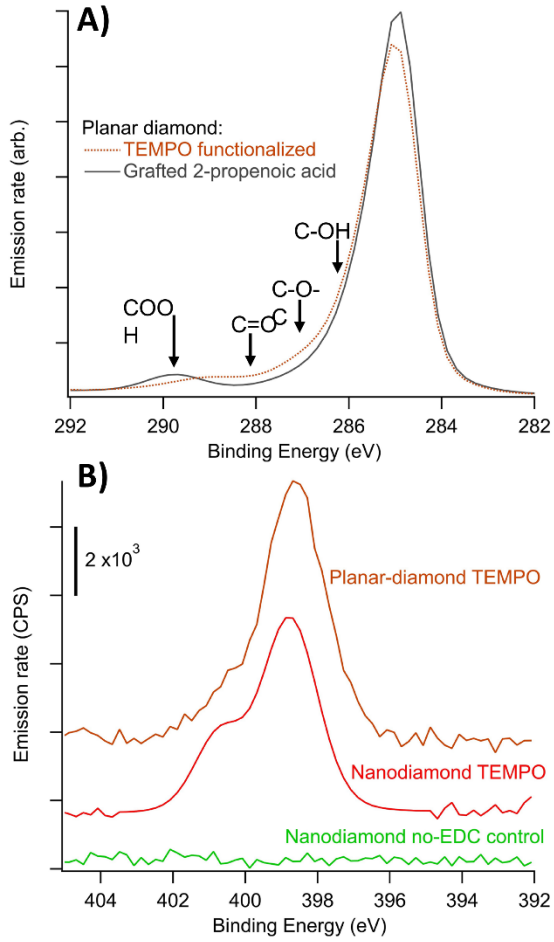

Figure 3: *XPS analysis of functionalized diamond samples. A) The C(1s) peaks of carboxylate-grafted HPHT planar diamond samples before and after TEMPO-functionalization normalized by peak area. B) The N(1s) peak of 2-propenoic acid grafted TEMPO-functionalized planar-diamond and nanodiamond samples with a nanodiamond no-EDC control.*

Fig. 4 shows the area density of grafted TEMPO molecules that we infer by integrating the C(1s) and N(1s) peak areas produced by the different linker molecules, and translating that into absolute coverages as described in the SI. We list the ratio of carboxylate to total C(1s) XPS signal rather than use the O(1s) emission because prior studies have shown that hydrophilic surfaces exposed to air readily acquire layers of physisorbed water, leading to large sample-dependent O(1) emission that is not directly associated with C-O bond formation; this leads to over-estimation of the true extent of surface oxidation when using O(1). [31] Fig. 4 plots the ratio of carboxylate signal to total C(1s) signal (estimated from C(1s) peak area associated with oxidized carbon) of nanodiamond before TEMPO functionalization against the TEMPO coverage of the same diamond after TEMPO functionalization (estimated from the N(1s) peak area). The strong linear correlation ($R^2 = 0.917$) between the percent of C1s signal in the carboxylate region (~289 eV) and the subsequent TEMPO coverage demonstrates the efficacy of the EDC crosscoupling reaction used here to bind TEMPO to exposed carboxylate groups. Data comparing the different chain lengths suggest that the coverage may be lower for the longest chain lengths, ranging from 0.7 to 1.8 molecules nm^{-2} as the linker length is increased. Also shown in Fig. 4 are the XPS data from a planar diamond sample. The planar sample shows a TEMPO density of 3.3 molecules nm^{-2}; that is higher than the highest densities observed from the nanodiamond samples. The origin of this difference is not known, but may be associated with differences in sample handling of nanoparticles vs. planar samples.

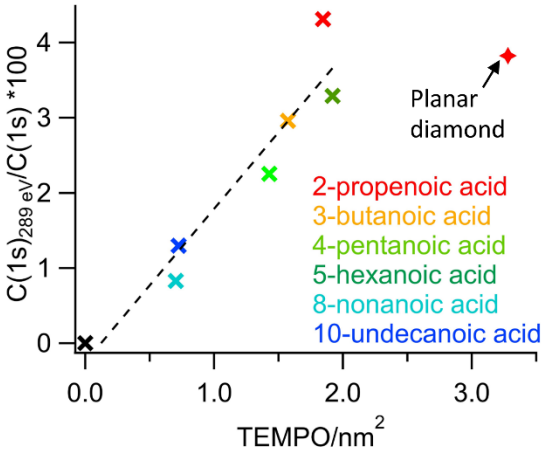

Figure 4: *XPS analysis of nano-diamond samples and HTHP planar diamond grafted with carboxylate groups and functionalized with TEMPO. The ratio of integrated C(1s) emission intensity in the carboxylate region near 289 nm to that obtaind from integrating the entire C(1s) region is indicative of the grafting density of each carboxylic acid. TEMPO coverage of the same samples after functionalization with TEMPO is estimated from the ratio N(1s)/C(1s) signal.*

3.3 Influence of air-annealing nanodiamond:

Recent studies have suggested that nanodiamond surfaces may contain significant amounts of sp^2-hybridized carbon that could influence the surface chemistry and the dynamics of near-surface spin centers, such as shallow-implanted NV centers and the surface-linked TEMPO molecules investigated here.[21] Prior work on radical-initiated grafting of organic compounds to H-terminated diamond was conducted on samples that were not air-annealed prior to H-termination.[17] To determine whether air-annealing prior to H-termination affects the subsequent functionalization reactions, we compared the properties of functionalized samples prepared with and without air annealing prior to the H-termination, using dynamic light scattering, XPS, DRIFTS, and EPR. Fig. 5 shows ZP data collected on non-annealed nanodiamond samples with an initial H-termination followed by subesquent surface modifications, measured under the same conditions as the air-annealed diamond shown in Fig 2.

Comparing Fig. 2 to Fig. 5 shows that the ZP of the starting H-terminated nanodiamond that was air-annealed prior to H-termination (+18 mV) is less positive than that of the sample that was not air annealed (+40 mV). The nanodiamond that was air-annealed before H-termination reaches a steady ZP faster (within ~ 30 minutes) and reaches a more negative value (ZP ~ -39 mV) compared with the non-annealed sample (~ 4 h reaction time, ZP ~ -30 mV). We also measured the DRIFTS and XPS spectra of both H-terminated air-annealed and non-annealed samples (see SI figures S3 and S4) and found that samples air-annealed prior to H-termination contain larger quantities of O-groups. It is unclear why the ZP of non-annealed nanodiamond samples grafted with ethenyl-terminated carboxylic acids for less than two-hours becomes negative after exposure to the TEMPO solution without EDC.

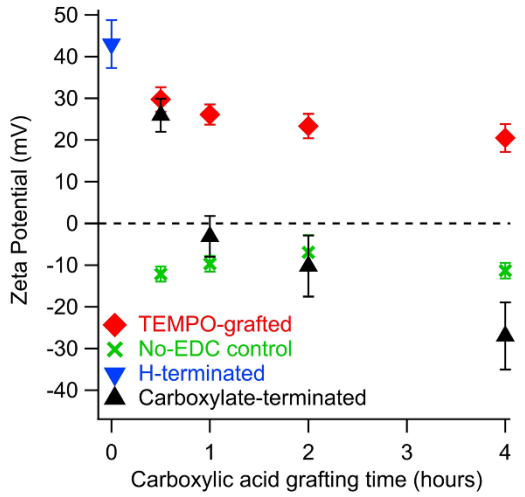

Figure 5: *Variation in zeta-potential of H-terminated nanodiamond without a prior air-anneal as a function of the duration of initial grafting of 10-undecenoic acid. Carboxylate-functionalized samples were then exposed to an aqueous solution of 4-amino-TEMPO with and without the EDC linker.*

Fig. 6 plots the single-integrated EPR spectra of dry, H-terminated nanodiamond both with and without a prior anneal in air. Because diamond has several bulk and surface defects that

are EPR-active, there are several peaks that arise from the diamond itself. [32-33] The three most abundant defects of nanodiamond this size are the substitutional nitrogen defects (P1 centers) and two surface carbon defects (frequently denoted SC1/SC2 or "X" in the literature) that are unique to nanodiamonds. [33-34] These surface defects have been attributed to negatively charged vacancy defects, "dangling bonds" in sp^2-hybridized carbon, and structural defects.[34-36] These two surface defects appear as only one peak at the X-band frequencies used here.[37] In Fig. 6, black arrows mark the location of the bulk P1 centers and the combined "surface defect" signal. While the detailed origins of these surface defects remain uncertain, our data in Fig. 6 show that the mass-normalized intensity of their EPR features decreases upon annealing in air, while the contribution from the P1 centers remains nearly unaffected. This result demonstrates that air-annealing reduces the concentration of spin-active surface defects.

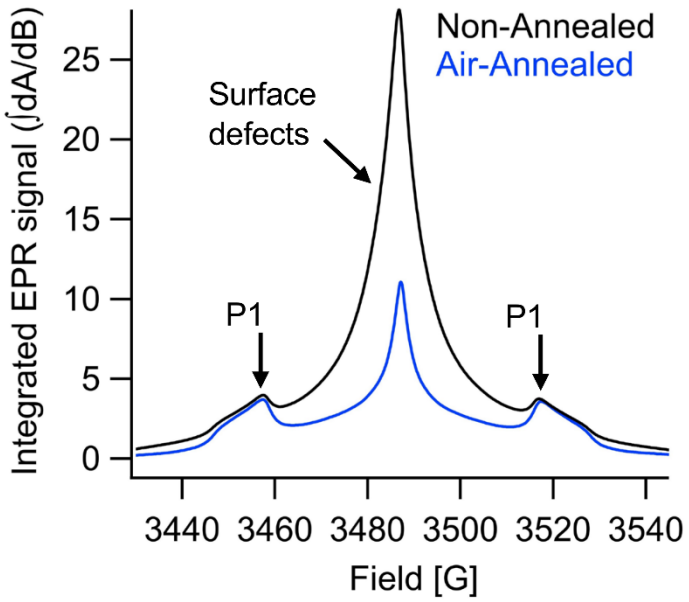

Figure 6: *Integrated EPR signal of dry H-terminated non-anneaeld (as-received) nanodiamond and air-annealed nanodiamond normalized by nanodiamond mass.*

3.4 EPR analysis of aminoxyl-radicals on nanodiamond

After TEMPO is grafted to nanodiamond, EPR features arising from aminoxyl-radicals and from diamond-based defects are both visible. Fig. 7 shows EPR spectra of nanodiamond samples that were grafted with TEMPO (TEMPO-ND) using 2-pentenoic acid as described above. EPR spectra of aminoxyl-radicals are strongly dependent on the mobility of the molecule, with restricted motion limiting isotropic averaging, and thereby causing broadening of the spectra.[38-39] To demonstrate the influence of measurement conditions on the spectra, we show spectra of TEMPO-functionalized nanodiamond measured as dry powders, measured after addition of 4 μL H_2O to hydrate the surface, and after addition of 8 μL H_2O with ultrasonic agitation to hydrate and break up aggregates. We also include a "No-EDC" control sample prepared identically except that no EDC was present to crosslink the TEMPO to the diamond surface during the functionalization step. While EPR spectra are typically acquired in derivative mode, single integration of the EPR signal yields peaks, while double-integration yields the total spin-signal from each sample.[33] To facilitate analysis of the spectra, we normalized the intensities of the spectra in Fig. 7 such that each spectrum has the same total double-integrated peak area.[33] Fig. 7 shows the EPR spectrum of TEMPO-ND in dry form; the three peaks corresponding to spin of aminoxyl radicals anisotropically oriented along the applied magnetic field and showing the greatest spectral width are denoted by the blue arrows. [38-39] Upon addition of a small amount of water to hydrate the sample, the peaks become more obvious, which we attribute to sharpening of the lines as a result of increased orientational averaging of the TEMPO molecules with greater rotational freedom. After the sample has additional water added and is ultrasonically agitated, these peaks become markedly sharper as the TEMPO can more easily reorient and the spins become more isotopically averaged, yielding the peaks indicated by the red arrows in Fig. 7.[38] Thus our experiments show that surface-tethered TEMPO molecules can be

readily detected by EPR, with line shapes that are dependent on the extent of hydration and the degree of aggregation.

Our data suggest that NP aggregation can play an important role in the EPR data. ZP measurements (SI, Fig. S6) show that under conditions where the EPR line shapes are sharpest, the ZP is also the most negative. These data suggest that higher colloidal stability leads to greater hydration of the primary nanoparticles and allows the largest fraction of surface-bound TEMPO to be fully hydrated. While not reported here in detail, extensive ultrasonication can also lead to mechanical disruption of the surface layers. Thus, optimum conditions for preparing and processing TEMPO-functionalized nanoparticles need to be chosen carefully. Measurements as wet slurries provide sharp peaks but retain some inhomogeneous peak shapes due to varying degrees of rotational freedom, which limits the ability to extract more detailed information by deconvolution or other numerical methods. Measurements as wet slurries also enable an approximate sample calibration via EPR by comparing the functionalized nanodiamond samples with an aqueous solution of TEMPO of known concentration and identical volume. [40]

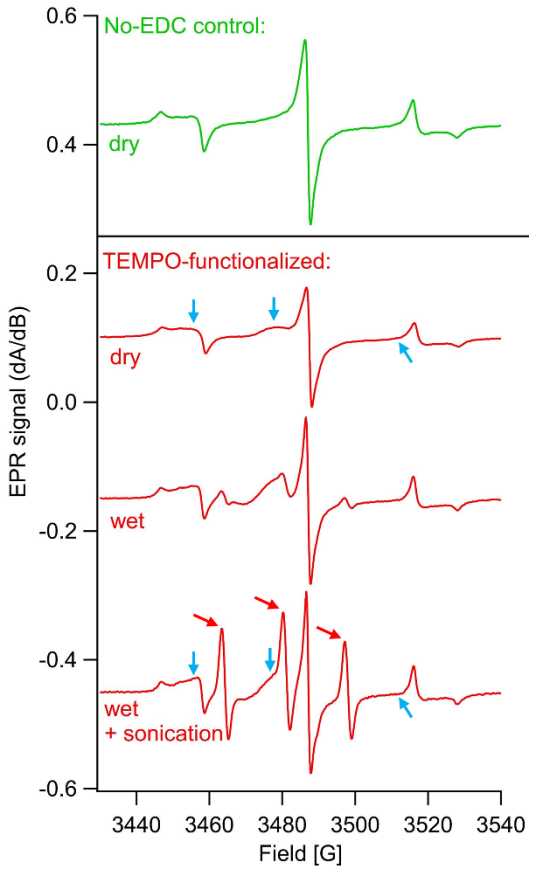

***Figure** 7: EPR spectra of 2-propenoic acid grafted nanodiamond samples normalized by total double-integrated signal intensity. From top to bottom: no-EDC control sample measured dry, TEMPO-ND measured dry, TEMPO-ND measured with 4 µL H_2O, TEMPO-ND measured with 8 µL and ultrasonicated for 30 seconds at 20.5 W power. Peaks associated with aminoxyl radicals are highlighted with arrows.*

To demonstrate the versatility of the above TEMPO grafting scheme, we functionalized nanodiamond samples using carboxylic acid precursors with different lengths of the hydrocarbon chain. To quantify the surface coverage of aminoxyl-radicals on our nanodiamond, we developed a procedure for quantifying the intensity of the EPR signal from the spin-active TEMPO signal in the presence of background signals from nanodiamond based on using factor analysis to isolate the contribution from TEMPO. This method is based on two important observations.

First, Fig. 8B shows that mass-normalized EPR from different "No-EDC Control" samples overlap almost perfectly in the region of P1 centers; this overlap demonstrates that in the absence of TEMPO, the surface functionalization procedure produces samples in which the background signal in the region of the TEMPO peaks (primarily from P1 centers located in the interior of the nanodiamond) is independent of the initial carboxylic acid used. Secondly, while the TEMPO peaks are in the same spectral region as P1 centers, the TEMPO features have a narrower spectral range. As a result, EPR spectra obtained using different masses of nanodiamond can be normalized by using the intensity of EPR signals in the wings of the P1 centers (outside the location of the TEMPO features) as an internal standard. This region is highlighted in yellow in Fig. 8. In order to estimate TEMPO coverages from EPR data, we performed an approximate calibration by measuring an air-annealed nanodiamond sample with known specific surface area and a second calibration by measuring a series of aqueous TEMPO solutions of known concentrations and comparing these standards with functionalized samples. . Using these values allowed us to quantitatively estimate the surface coverage of TEMPO molecules from the EPR measurements. Details of these procedures are presented in the SI.

Using the above quantification procedure, we measured the intensity of the TEMPO EPR signal from nanodiamonds functionalized via carboxylic acid linkers of different lengths. Fig. 8A and 8B show the normalized EPR spectra that were then quantified as described above. Fig. 8C shows the resulting surface area density of aminoxyl radicals from TEMPO. Our result shows that the aminoxyl-radical coverage is nearly equivalent for all samples, visual inspection suggests that there may be a small decrease in surface coverage with increasing linker length, but statistical analysis indicates that this decrease is within the uncertainty and therefore is not verified . We further quantified the surface nitrogen concentration using independent

measurements from X-ray photoelectron spectroscopy as described above. The absolute quantification via each method has significant systematic error associated with the different calibration steps involved; nevertheless, it shows that both techniques are able to effectively probe the efficiency of grafting of TEMPO.

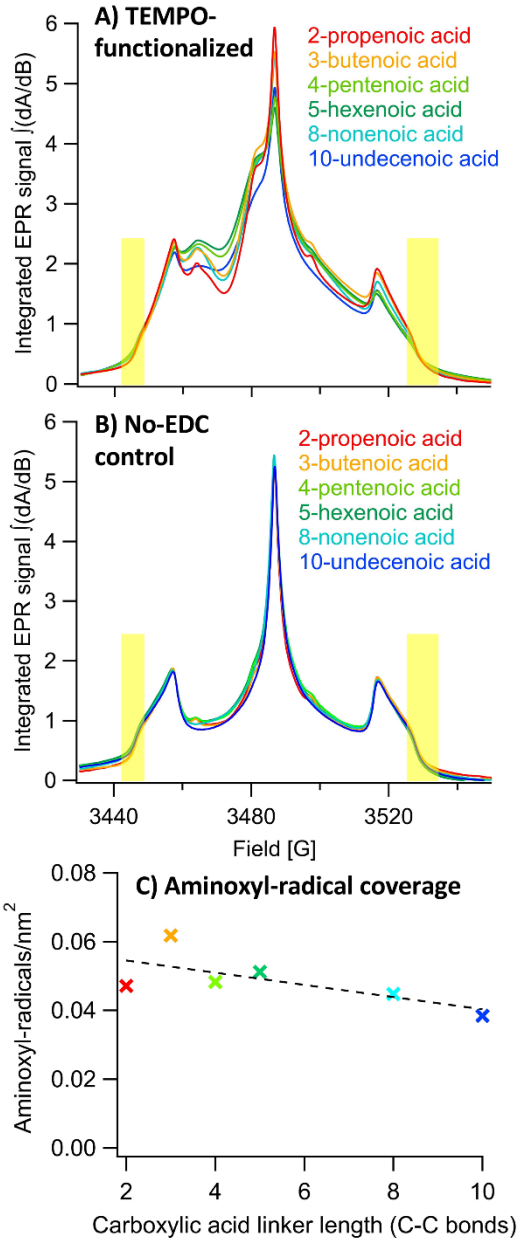

Figure 8: *Quanfication of aminoxyl-radical surface coverage of nanodiamond by EPR.* ***A)*** *TEMPO-functionalized diamond in 4 µL water normalized by the average signal intensity in the*

highlighted area. ***B)*** *No-EDC control samples of nanodiamond in 4 µL water normalized by the average signal intensity in the highlighted area.* ***C)*** *Aminoxyl-radical surface coverage calculated verses acid-linker length. The dashed shows a linear fit suggesting a possible downward trend but this decresae is not statisically validated at a 95% confidence level.*

3.5 Applications and quantification

Overall, the results above demonstrate the ability to prepare diamond samples functionalized with spin-active aminoxyl radicals via surface tethers of different lengths. A strong motivation for this work is the rapidly advancing area of quantum chemical sensing, in which spin-spin interactions between sub-surface nitrogen-vacancy (NV) centers and chemical probe molecules (such as TEMPO) forms the basis of new types of chemical and biological sensors.[41] For these emerging fields to advance, it is important to have good control over the surface species and to be able to prepare surfaces with well-defined densities of spin-active centers at well-controlled distances from the diamond itself. The approach outlined here provides that controllability and is shown here to be applicable to both bulk diamond and nanodiamond. Quantum sensing studies typically use NV centers implanted 5-10 nm beneath the surface of a bulk diamond sample.[41] Because dipolar spin-spin interactions extend a distance of ~ 10 nm, interaction between buried NV centers and surface spins will be greatest when the lateral distance between surface spins is comparable to or less than the depth of the spins beneath the surface. [42] Our results show that use of radical grafting combined with EDC functionalization can produce surfaces with covalently linked, spin-active TEMPO with molecular densities up to ~ 0.1 molecule/nm^2, or an average distance of <10 nm between adjacent TEMPO molecules.

Our data shows that there is a linear relationship between the surface density of TEMPO molecules measured by XPS and the aminoxyl-radical coverage as measured by EPR (R^2 = 0.67). However, the surface densities inferred from the EPR measurements are lower than those estimated from XPS. The most likely origin of this difference is that aggregation of the nanodiamond before or during functionalization likely leads to interior regions of the aggregates being less accessible to functionalization compared to the outermost surfaces of the aggregates. To extract a surface coverage from EPR, it is necessary to know the specific surface area. In measurements reported above we used surface area measured by BET, with typical values of 46 m^2/g. However, BET measures the total surface area including interstitial regions that maybe inaccessible to functionalization in liquids , and therefore likely under-estimates the actual TEMPO area density. If we instead use the nanoparticle size distribution from DLS and the known mass, we obtain a typical specific surface area of ~ 7.4 m^2/g, lower than that obtained by BET since DLS reflects the size of the exterior of the nanoparticle and its bound hydration layer. (see SI Fig. 6). If we estimate the surface coverage of spin-active TEMPO density using the specific surface area inferred from DLS, we obtain typical coverages between 0.4 - 0.5 aminoxyl radicals/nm^2, much closer to the value of 0.7 – 1.9 molecules/nm^2 measured by XPS using different-lenth linkers on nanodiamond. Based on these results, we conclude that both XPS and EPR show that our functionalization chemistry yields surface densities on the order of 0.5 spin-active TEMPO molecule/nm^2 from those regions of the sample that are accessible (e.g., the outermost regions of the nanodiamond aggregates). Irrespective of which surface area measurement is used, the TEMPO coverages we obtain are higher than the values of 0.003 – 0.01 aminoxyl-radicals/nm^2. reported previously using alternative functionalization methods (and inferring surface area from DLS). [7-8] Due to experimental limitations, we were unable to measure

our planar diamond by EPR, but as aggregation is not possible on the planar surface, we would not expect significant deviation between the TEMPO surface coverage estimated by XPS and EPR.

Defects in the bulk and on the surface of diamond reduce the quantum coherence time of shallow NV centers, decreasing the sensitivity to surface-tethered radical species such as TEMPO.[19] We have demonstrated the grafting of carboxylate groups to H-terminated diamond both with and without a prior anneal in air, a process that decreases the concentration of adventitious surface radials on nanodiamond. During grafting of the carboxylic acid, the ZP of nanodiamonds that are air-annealed prior to H-termination reach a stable value faster than non-annealed samples. We hypothesize that this faster grafting rate to may be due to an orientation effect, with carboxylate groups more weakly-coordinating to the less-positive ZP surface, increasing the contact of the ethenyl-groups to surface radicals.[43] However, there may be other explanations including influence by surface sp^2 carbon or aggregation due the different ZP. After functionalization with TEMPO using the EDC crosslinker, the ZP of the nanodiamond increases by ~45 mV in both air-annealed and non-annealed nanodiamond. This significant positive shift in ZP indicates the removal of surface carboxylate groups and suggests that the H-termination is preserved between grafted molecules. Our XPS analysis of carboxylate terminated diamond suggests the same result because within experimental uncertainty, no non-carboxylate species can be detected on the diamond surface.

CONCLUSIONS

Our results demonstrate a highly scalable and controllable approach to functionalization of diamond with spin-active functional groups through stable amide bonds using radical-initiated grafting of ethenyl-terminated carboxylic acids to H-terminated diamond. The ability to link

TEMPO and related spin-active molecules to surfaces of nanoparticle and planar diamond is important because it provides a pathway to novel types of quantum-based chemical sensing that make use of interactions between sub-surface quantum defects (e.g., NV centers) and surface-bound spin-active molecules. We demonstrate that this chemistry works on nanodiamond with a pre-treatment of air-annealing that reduces the number of surface-radicals that may interfere with coherence measurements between shallow defects and functionalized radical species. [21] Our data show that radical-induced grafting of ethenyl-terminated carboxylic acids leads to surface coverages of carboxylate groups comparable to those produced by oxidation by hot mineral acids and gives the ability to control the length of the molecular linker between the diamond surface and the TEMPO spin probe. [8, 11] Our studies yield estimated surface densities of 4-amino-TEMPO of approximately 1.4 molecules nm^{-2} on nanodiamond (varying with molecular linker length) and 3.3 molecules nm-^{2} on planar diamond. These surface coverage values are significantly greater than those reported previously using different functionalized schemes.[8] When using nanodiamond, aggregation may leads to higher TEMPO densities on the exposed exterior surfaces (as probed by XPS) and lower TEMPO densities in the interstitial regions of the aggregates. This work provides a general approach to multi-step surface chemistry of TEMPO and other delicate molecules that may be attractive candidates for applications such as chemical sensing.

ASSOCIATED CONTENT

Details of diamond preparation. Quantification via TEMPO coverage via XPS. Normalization of EPR data. Infrared spectroscopy of nanodiamond and influence of air-annealing. This material is available free of charge via the Internet at http://pubs.acs.org

AUTHOR INFORMATION

Corresponding Author

rjhamers@wisc.edu
ORCID:
Benjamin F. Bachman: 0000-0002-1356-0387
Zachary R. Jones: 0000-0001-8725-975X
Gabriel R. Jaffe 0000-0003-2672-0375
Jad Salman 0000-0002-2365-3667
Ray Wambold 0000-0002-3536-7940
Zhaoning April Yu: 0000-0002-8041-0004
Jennifer T. Choy 0000-0002-8689-3801
Shimon J. Kolkowitz: 0000-0001-7095-1547
Mark A. Eriksson: 0000-0002-3130-9735
Mikhail A. Kats 0000-0003-4897-4720
Robert J. Hamers 0000-0003-3821-9625

Notes
The authors declare no competing financial interest.

ACKNOWLEDGMENT

This work was supported by the National Science Foundation CHE1839174. XPS studies were conducted at the UW-Madison Materials Science Center, which is partially supported by the University of Wisconsin Materials Research Science and Engineering Center (DMR-1720415). Additional contributions by JTC and SK were supported by the U.S. Department of Energy (DOE), Office of Science, Basic Energy Sciences (BES) under Award #DE- SC0020313. We would like to gratefully acknowledge Dr. Heike Hofstetter for helpful discussions.

REFERENCES

1. May, P. W., Diamond thin films: A 21st-century material. *Philos. Trans. R. Soc. Lond. Ser. A-Math. Phys. Eng. Sci.* **2000,** *358*, 473-495.

2. Zhu, D.; Zhang, L. H.; Ruther, R. E.; Hamers, R. J., Photo-illuminated diamond as a solid-state source of solvated electrons in water for nitrogen reduction. *Nature Mater.* **2013,** *12*, 836-841.

3. Raymakers, J.; Haenen, K.; Maes, W., Diamond surface functionalization: From gemstone to photoelectrochemical applications. *J. Mater. Chem. C* **2019,** *7*, 10134-10165.

4. Yang, W. S.; Auciello, O.; Butler, J. E.; Cai, W.; Carlisle, J. A.; Gerbi, J.; Gruen, D. M.; Knickerbocker, T.; Lasseter, T. L.; Russell, J. N.; Smith, L. M.; Hamers, R. J., DNA-modified nanocrystalline diamond thin-films as stable, biologically active substrates. *Nature Materials* **2002,** *1*, 253-257.

5. Stavis, C.; Clare, T. L.; Butler, J. E.; Radadia, A. D.; Carr, R.; Zeng, H. J.; King, W. P.; Carlisle, J. A.; Aksimentiev, A.; Bashir, R.; Hamers, R. J., Surface functionalization of thin-film diamond for highly stable and selective biological interfaces. *Proc. Natl. Acad. Sci. U. S. A.* **2011,** *108*, 983-988.

6. Sun, B.; Colavita, P. E.; Kim, H.; Lockett, M.; Marcus, M. S.; Smith, L. M.; Hamers, R. J., Covalent photochemical functionalization of amorphous carbon thin films for integrated real-time biosensing. *Langmuir* **2006,** *22*, 9598-9605.

7. Barton, J.; Gulka, M.; Tarabek, J.; Mindarava, Y.; Wang, Z. Y.; Schimer, J.; Raabova, H.; Bednar, J.; Plenio, M. B.; Jelezko, F.; Nesladek, M.; Cigler, P., Nanoscale dynamic readout of a chemical redox process using radicals coupled with nitrogen-vacancy centers in nanodiamonds. *ACS Nano* **2020,** *14*, 12938-12950.

8. Romanova, E. E.; Akiel, R.; Cho, F. H.; Takahashi, S., Grafting nitroxide radicals on nanodiamond surface using click chemistry. *J. Phys. Chem. A* **2013,** *117*, 11933-11939.

9. Jones, Z. R.; Niemuth, N. J.; Robinson, M. E.; Shenderova, O. A.; Klaper, R. D.; Hamers, R. J., Selective imaging of diamond nanoparticles within complex matrices using magnetically induced fluorescence contrast. *Environ.-Sci. Nano* **2020,** *7*, 525-534.

10. Jelezko, F.; Wrachtrup, J., Single defect centres in diamond: A review. *Phys. Status Solidi A-Appl. Mat.* **2006,** *203*, 3207-3225.

11. Wang, X. F.; Ruslinda, A. R.; Ishiyama, Y.; Ishii, Y.; Kawarada, H., Higher coverage of carboxylic acid groups on oxidized single crystal diamond (001). *Diamond and Related Materials* **2011,** *20*, 1319-1324.

12. Tokuda, N.; Umezawa, H.; Ri, S. G.; Yamabe, K.; Okushi, H.; Yamasaki, S., Roughening of atomically flat diamond (111) surfaces by a hot HNO_3/H_2SO_4 solution. *Diam. Relat. Mater.* **2008,** *17*, 486-488.

13. Thoms, B. D.; Owens, M. S.; Butler, J. E.; Spiro, C., Production and characterization of smooth, hydrogen-terminated diamond C(100). *Appl. Phys. Lett.* **1994,** *65*, 2957-2959.

14. John, P.; Stoikou, M. D., Hydrogen plasma interaction with (100) diamond surfaces. *Phys. Chem. Chem. Phys.* **2011,** *13*, 11503-11510.

15. Seshan, V.; Ullien, D.; Castellanos-Gomez, A.; Sachdeva, S.; Murthy, D. H. K.; Savenije, T. J.; Ahmad, H. A.; Nunney, T. S.; Janssens, S. D.; Haenen, K.; Nesladek, M.; van der Zant, H. S. J.; Sudholter, E. J. R.; de Smet, L., Hydrogen termination of CVD diamond films by high-temperature annealing at atmospheric pressure. *J. Chem. Phys.* **2013,** *138*, 234707.

16. Strother, T.; Knickerbocker, T.; Russell, J. N.; Butler, J. E.; Smith, L. M.; Hamers, R. J., Photochemical functionalization of diamond films. *Langmuir* **2002,** *18*, 968-971.

17. Zhang, Y. Q.; Tamijani, A. A.; Taylor, M. E.; Zhi, B.; Haynes, C. L.; Mason, S. E.; Hamers, R. J., Molecular surface functionalization of carbon materials via radical-induced grafting of terminal alkenes. *J. Am. Chem. Soc.* **2019,** *141*, 8277-8288.

18. Ida, S.; Tsubota, T.; Tanii, S.; Nagata, M.; Matsumoto, Y., Chemical modification of the diamond surface using benzoyl peroxide and dicarboxylic acids. *Langmuir* **2003,** *19*, 9693-9698.

19. Kumar, R.; Singh, D. K.; Kumar, P.; Kumar, R.; Dhakate, S. R., Influence of degree of air oxidation and functionality on ensemble emission from nitrogen vacancy centers in nano-diamonds. *Diam. Relat. Mater.* **2019,** *97*, 107431.

20. Osswald, S.; Yushin, G.; Mochalin, V.; Kucheyev, S. O.; Gogotsi, Y., Control of $sp^{2/}sp^3$ carbon ratio and surface chemistry of nanodiamond powders by selective oxidation in air. *J. Am. Chem. Soc.* **2006,** *128*, 11635-11642.

21. Stacey, A.; Dontschuk, N.; Chou, J. P.; Broadway, D. A.; Schenk, A. K.; Sear, M. J.; Tetienne, J. P.; Hoffman, A.; Prawer, S.; Pakes, C. I.; Tadich, A.; de Leon, N. P.; Gali, A.; Hollenberg, L. C. L., Evidence for primal sp^2 defects at the diamond surface: Candidates for electron trapping and noise sources. *Adv. Mater. Interfaces* **2019,** *6*, 1801449.

22. Laube, C.; Riyad, Y. M.; Lotnyk, A.; Lohmann, F. P.; Kranert, C.; Hermann, R.; Knolle, W.; Oeckinghaus, T.; Reuter, R.; Denisenko, A.; Kahnt, A.; Abel, B., Defined functionality and increased luminescence of nanodiamonds for sensing and diagnostic applications by targeted high temperature reactions and electron beam irradiation. *Mater. Chem. Frontiers* **2017,** *1*, 2527-2540.

23. Wolcott, A.; Schiros, T.; Trusheim, M. E.; Chen, E. H.; Nordlund, D.; Diaz, R. E.; Gaathon, O.; Englund, D.; Owen, J. S., Surface structure of aerobically oxidized diamond nanocrystals. *J. Phys. Chem. C* **2014,** *118*, 26695-26702.

24. Nozaki, K.; Bartlett, P. D., The kinetics of decomposition of benzoyl peroxide in solvents .1. *J. Am. Chem. Soc.* **1946,** *68*, 1686-1692.

25. Uchida, T.; Hamano, A.; Kawashima, N.; Takeuchi, S., Disaggregation and surface modification of nano-size diamond by ultrasound exposure: Relationships among acoustic

intensity, disaggregation, and surface modification. *Electron. Commun. Jpn. Pt. III-Fundam. Electron. Sci.* **2007,** *90*, 10-18.

26. *CasaXPS, version* 2.3.23PR1.0; Casa Software Ltd, 2020.

27. Swift, P., Adventitious carbon - the panacea for energy referencing. *Surf. Interfac. Analysis* **1982,** *4*, 47-51.

28. Gines, L.; Mandal, S.; Ashek, I. A.; Cheng, C. L.; Sow, M.; Williams, O. A., Positive zeta potential of nanodiamonds. *Nanoscale* **2017,** *9*, 12549-12555.

29. Day, A. H.; Adams, S. J.; Gines, L.; Williams, O. A.; Johnson, B. R. G.; Fallis, I. A.; Loveridge, E. J.; Bahra, G. S.; Oyston, P. C. F.; Herrera, J. M.; Pope, S. J. A., Synthetic routes, characterization and photophysical properties of luminescent, surface functionalized nanodiamonds. *Carbon* **2019,** *152*, 335-343.

30. Desimoni, E.; Casella, G. I.; Morone, A.; Salvi, A. M., XPS determination of oxygen-containing functional-groups on carbon-fiber surfaces and the cleaning of these surfaces. *Surf. Interfac. Analysis* **1990,** *15*, 627-634.

31. Kwoka, M.; Krzywiecki, M., Impact of air exposure and annealing on the chemical and electronic properties of the surface of SnO_2 nanolayers deposited by rheotaxial growth and vacuum oxidation. *Beilstein J. Nanotechnol.* **2017,** *8*, 514-521.

32. Zegrya, G. G.; Samosvat, D. M.; Osipov, V. Y.; Vul, A. Y.; Shames, A. I., Size effect in electron paramagnetic resonance spectra of impurity centers in diamond nanoparticles. *arXiv:1912.06330.* **2019**.

33. Yavkin, B.; Gafurov, M.; Volodin, M.; Mamin, G.; Orlinskii, S. B., Epr and double resonances in study of diamonds and nanodiamonds, *Experimental Methods in Physical Sciences* **2019**, *50,* 83-113.

34. Peng, Z.; Biktagirov, T.; Cho, F. H.; Gerstmann, U.; Takahashi, S., Investigation of near-surface defects of nanodiamonds by high-frequency EPR and DFT calculation. *J. Chem. Phys.* **2019,** *150*, 134702.

35. Osipov, V. Y.; Shames, A. I.; Vul, A. Y., Exchange coupled pairs of dangling bond spins as a new type of paramagnetic defects in nanodiamonds. *Physica B: Condensed Matter* **2009,** *404*, 4522-4524.

36. Fang, X.; Mao, J.; Levin, E. M.; Schmidt-Rohr, K., Nonaromatic core-shell structure of nanodiamond from solid-state nmr spectroscopy. *J. Am. Chem. Soc.* **2009,** *131*, 1426-1435.

37. Yavkin, B. V.; Mamin, G. V.; Gafurov, M. R.; Orlinskii, S. B., Size-dependent concentration of n-0 paramagnetic centres in hpht nanodiamonds. *Magn. Reson. Solids* **2015,** *17*, 15101.

38. Santangelo, M. G.; Levantino, M.; Cupane, A.; Jeschke, G., Solvation of a probe molecule by fluid supercooled water in a hydrogel at 200 K. *J. Phys. Chem. B* **2008,** *112*, 15546-15553.

39. Clark, A.; Sedhom, J.; Elajaili, H.; Eaton, G. R.; Eaton, S. S., Dependence of electron paramagnetic resonance spectral lineshapes on molecular tumbling: Nitroxide radical in water: Glycerol mixtures. *Concepts Magn. Reson. Part A* **2016,** *45A*, 21423.

40. Owenius, R.; Engstrom, M.; Lindgren, M.; Huber, M., Influence of solvent polarity and hydrogen bonding on the EPR parameters of a nitroxide spin label studied by 9-GHz and 95-GHz EPR spectroscopy and DFT calculations. *J. Phys. Chem. A* **2001,** *105*, 10967-10977.

41. Schirhagl, R.; Chang, K.; Loretz, M.; Degen, C. L., Nitrogen-vacancy centers in diamond: Nanoscale sensors for physics and biology. *Ann. Rev. Phys. Chem*. **2014,** *65,* 83-105.

42. Liu, H. B.; Plenio, M. B.; Cai, J. M., Scheme for detection of single-molecule radical pair reaction using spin in diamond. *Phys. Rev. Lett.* **2017,** *118*, 200402.

43. Hanaor, D.; Michelazzi, M.; Leonelli, C.; Sorrell, C. C., The effects of carboxylic acids on the aqueous dispersion and electrophoretic deposition of ZrO_2. *J. European Ceramic Soc.* **2012,** *32*, 235-244.

TOC figure (for publication only)

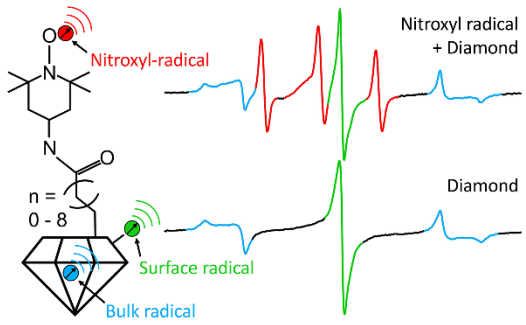

Supplemental information to

High-density covalent grafting of spin-active molecular moieties to diamond surfaces

Benjamin F. Bachman[†], Zachary R. Jones[†], Gabriel R. Jaffe[‡], Jad Salman[⊥], Raymond Wambold[⊥], Zhaoning Yu[‡,⊥], Jennifer T. Choy[§], Shimon J. Kolkowitz[‡], Mark A. Eriksson[‡], Mikhail A. Kats[‡,⊥], Robert J. Hamers[†]*

†Department of Chemistry, University of Wisconsin – Madison, 1101 University Avenue, Madison WI 53706

‡Department of Physics, University of Wisconsin – Madison, 1150 University Avenue, Madison WI 53706

⊥Department of Electrical and Computer Engineering, University of Wisconsin – Madison 1415 Engineering Drive, Madison, WI 53706

§Department of Engineering Physics, University of Wisconsin – Madison, 1500 Engineering Drive, Madison, WI 53706

Removal of surface graphitic contaminants:

Fig. S1: *H-terminated nanodiamond samples suspended in benzene solution in sealed crimp-vials. Left: air-annealed prior to H-termination. Right: sample was not air-annealed.*

Cleaning and preparation of nanodiamond samples

The nanodiamond functionalized with 2-propenoic acid, 3-butenoic acid, 4-pentenoic acid, 5-hexenoic acid, 8-nonenoic acid, and 10-undecenoic acid, are hereafter referred to as 2A, 3A, 4A, 5A, 8A, and 10A, respectively. After acid functionalizing and ultrasonicating, the functionalized diamond samples were transferred to 40 mL centrifuge tubes with the assistance of an acetone rinse, the 2A containing solution polymerized on contact with the acetone. Each subsequent rinsing step consisted of centrifugation at 4700xg for at least 10 minutes until the nanodiamonds formed a pellet, followed by resuspension in a solvent with a vortex mixer, followed by ultrasonication for 60 seconds at 21.5 W. The first rinsing step for all samples was 10 mL of acetone. 2A was vortexed but not sonicated when in acetone, as it was found in previous measurements to form a colloid that shows significant suspension even after 90 minutes of centrifugation at 4700xg. 8A and 10A both received an extra rinse with 10 mL of isopropyl alcohol (IPA) to help removed the excess acids that are sparingly soluble in water. For the 2nd rinsing step, 2A was suspended in 40 mL of water, 3A and 4A were suspended in a 40 mL

solution of water : acetone in a 3:1 ratio, and 5A, 8A, and 10A were suspended in a 40 mL solution of water : acetone in a 1:1 ratio. This tuning of the water: acetone ratio was meant to both reduce centrifugation times and to help remove the various acids of different solubilities. For the 3rd and 4th rinsing steps, all samples were suspended in 40 mL of water and centrifuged for 45 and 60 minutes, respectively. After the final rinsing step, the particles are suspended in 10 mL water and sonicated for 20 minutes each at 30 % power, to remove all visible aggregates. Particles are rinsed with a minimum of 130 mL of solution and 42 minutes of ultrasonication.

XPS quantification:

Surface coverages of TEMPO were calculated using the XPS coverage equation, shown in equation 1:

$$Coverage_{Element} = \frac{Area_{Element}}{Area_{C(1s)}} * \frac{SF_{C(1s)}}{SF_{Element}} * \frac{Scans_{C(1s)}}{Scans_{Element}} * \rho * \lambda * \cos(45°)$$

Where element areas are determined through peak integration using CasaXPS software after applying a Shirley background correction to baseline the peaks. Sensitivity factors (SF) used for C, N, S, Si, and O, were 1.0, 1.67615, 1.8809, 0.9, and 1.67615, respectively. Substrate density (ρ) was assumed to be 176 C atoms/nm^3, and the inelastic mean free path (λ) 1.9 nm. [1, 2]

To determine TEMPO surface coverage, an addition step of quantifying and subtracting the S signal contribution was done to remove the contribution to the N signal by adsorbed sulfo-NHS catalyst. To quantify O coverage, a similar subtraction of the Si signal was done to remove SiO_2 impurities, every Si was assumed to contribute two O atoms.

EPR normalization:

It is important to note our inability to completely remove the TEMPO signal at the rigid limit, as this broad and inhomogeneous signal overlap makes conventional methods of spectral deconvolution difficult to apply. We also found an unacceptable amount of error when

normalizing our nanodiamond samples by mass, due to the small volumes used. The first step of our surface density quantification method by EPR is to align all spectra by the zero-crossing of the surface-defect, followed by integration and baselining with a linear function. Second, the intensity of a dry air-annealed sample of known mass is divided by the average signal ratio of all samples both dry and wet to account for water-induced signal attenuation, a value of 2.87 ± 1.1 is used here. It should be noted that the procedure in the second step is done instead of using a wet calibration standard to account for the larger water : diamond ratio in the no-EDC control samples. Third, the average diamond signal intensity of each sample outside of the spectral range of TEMPO is used to normLized the spectra to the attenuation-corrected air-annealed standard of known mass. To determine the spectral range of diamond-only signal, principal component analysis was performed on all raw EPR data in order to separate the nanodiamond and TEMPO spectra using OriginPro software. Fig.S 2 shows the separated spectra as well as the ratio of the spectra; areas where the ratio is greater than or equal to 5 (denoted by the red line in Fig. S2) along the edges of the spectra are considered for our analysis to be diamond-only signal, this area is highlighted in yellow in fig. 7B of the main text.

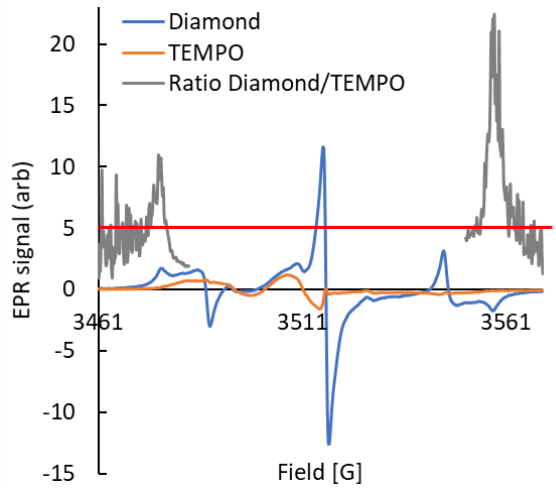

Fig. S2*: Diamond and TEMPO signal separated by principal component analysis. Areas where the ratio of diamond/TEMPO signal is greater than 5 are considered to be diamond-only.*

The signal of the normalized TEMPO-functionalized and no-EDC control samples are subtracted, and the remaining signal is converted to molecules of TEMPO using the calibration plotted in fig. S4. Finally, the mass of the diamond standard and BET surface area of H-terminated air-annealed diamond (46.5 m^2/g) is used to determine total surface area.

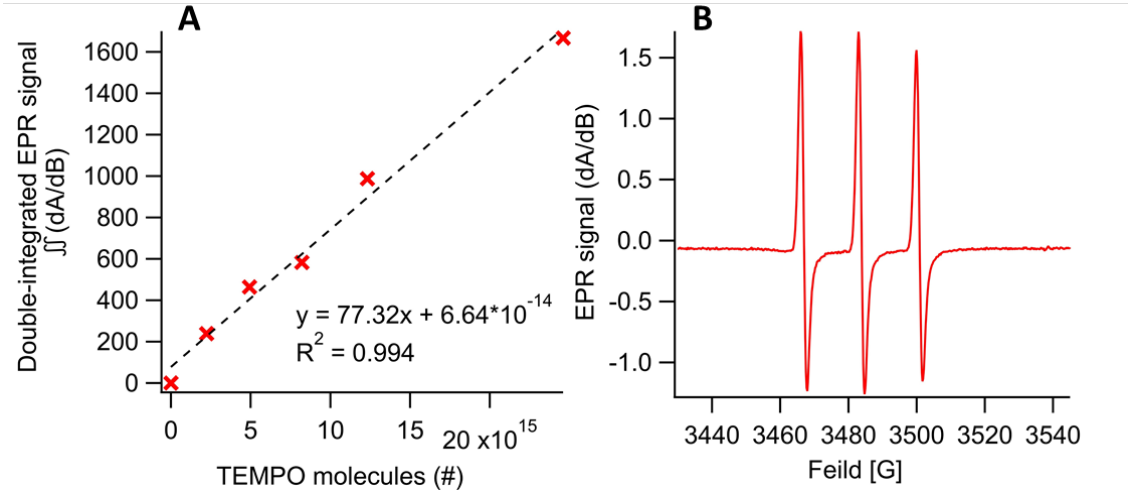

Fig. S3*: EPR TEMPO signal calibration in 4 µL H_2O. A) Simple linear regression fit to the total EPR signal of various TEMPO solutions at different concentrations. B) EPR spectra of a 3.4 mM aqueous solution of 4-amino-TEMPO.*

EPR uncertainty analysis:

The total uncertainty for the EPR analysis of nitroxyl-radical surface coverage on nanodiamond is 38.0 %. The four largest sources of experimental uncertainty contribute to this total value are listed below:

1. The standard error of the total EPR signal of the normalized no-EDC samples. This uncertainty arises from TEMPO remaining on the no-EDC diamond samples and small differences in sample preparation. Standard error is 2.6 %

2. The uncertainty in masses of both TEMPO and dry diamond standard contribute 0.8 and 1.1 % uncertainty respectively.
3. The differences in total normalized area of the no-EDC control indicates residual aminoxyl-radicals and leads to an underestimation of total radical coverage. Standard error = 4.25 %
4. The uncertainty introduced by water attenuation of the samples was determined by measuring the average signal reduction in of all TEMPO-functionalized samples after water was added to each. Average ratio of dry/wet signal: 2.9 ±1.1 Standard error = 37.6 %

DRIFTS of H-terminated nanodiamond with and without a prior air anneal:

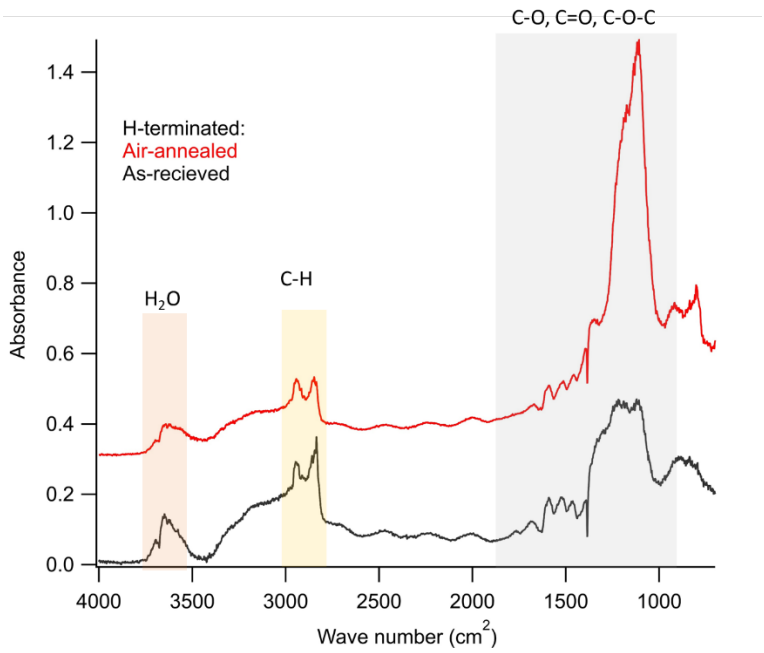

Fig. S4: *DRIFTS measurements of H-terminated nanodiamond with and without prior air-annealing. Samples preparation and peak assignments are from prior literature methods. [3]*

XPS survey spectrum of H-terminated nanodiamond with and without a prior air anneal:

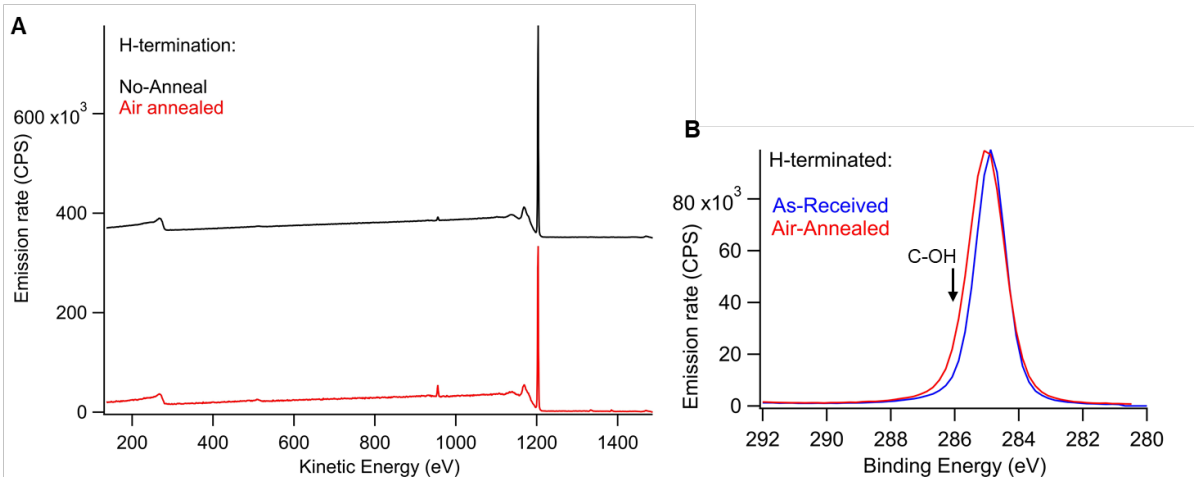

Fig. S5: *XPS analysis of H-terminated nanodiamond with and without prior air-annealing. A) Survey spectra of both nanodiamond samples. Emission from the underlying Si substrate is visible and is corrected for when quantifying O-surface coverage. The O-surface coverage of the H-terminated non-annealed and air-annealed samples is 0.15 and 0.34 O/nm^2 respectively. B) C(1s) signal of both nanodiamond samples. The air-annealed sample shows a wider C(1s) peak indicating the presence of oxidized surface carbons.*

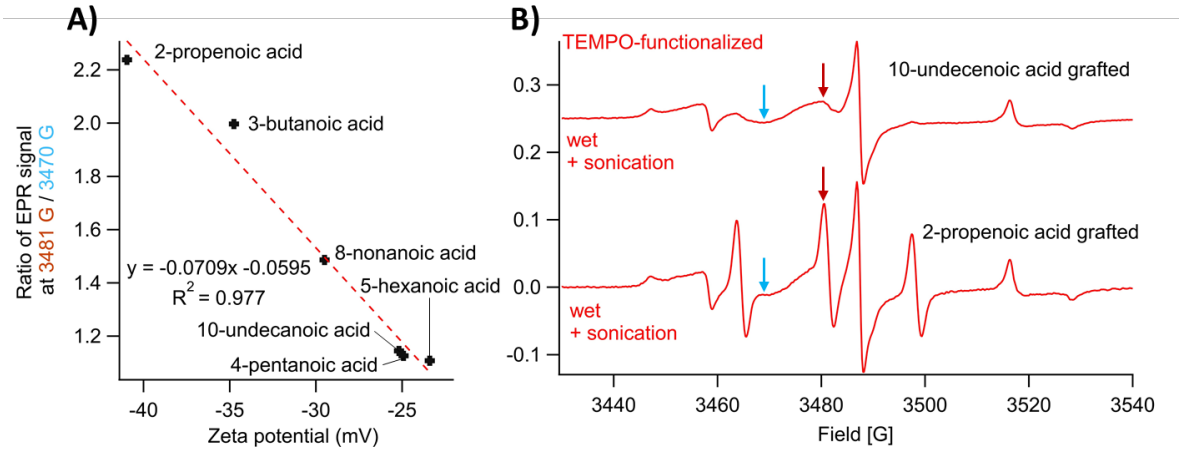

Fig. S6: *correlation between TEMPO in the tumbling-regime to ZP of nanodiamond after carboxylic acid grafting. This data suggests that the more colloidally stable nanoparticles show more freely rotating TEMPO. These samples were sonicated as described in the methods section.*

Hydrodynamic size analysis of functionalized nanodiamond:

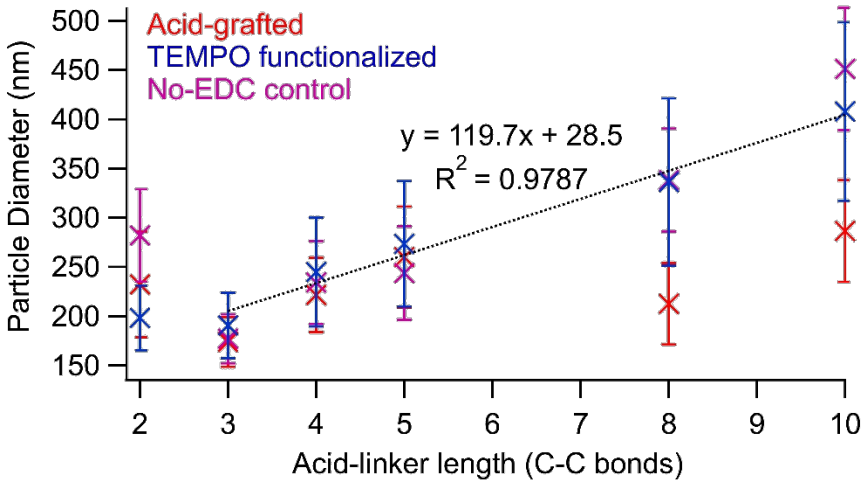

Fig.S7: *DLS analysis of nanodiamond aggregation after the final rinsing step of each functionalization. Samples were prepared as described in the materials and methods section, with the addition of a sonication step for 60 seconds at 21.5 W power before analysis. Acid-grafted nanodiamond are all the same within statistical uncertainty with the exception of samples functionalized with 3-butenoic acid and 10-undecanoic acid. A liner regression analysis is applied TEMPO-functionalized nanodiamond samples excluding the sample functionalized with 2-propenoic acid.*

REFERENCES:

1. Zhang, Y.Q.; Tamijani, A.A., Taylor, M.E. ; Zhi B.; Haynes, C.L.; Mason, S.E.; Hamers, R.J., *Molecular Surface Functionalization of Carbon Materials via Radical-Induced Grafting of Terminal Alkenes.* J. Am. Chem. Soc., **2019,** *141,* 8277-8288.
2. Tanuma, S., Powell, C.J.; Penn, D.R. *Calculations of electron inelastic mean free paths. IX. Data for 41 elemental solids over the 50 eV to 30 keV range.* Surf. Interfac. Analysis **2011**. *43*, 689-713.
3. Petit, T.; Puskar, L. *FTIR spectroscopy of nanodiamonds: Methods and interpretation.* Diamond and Related Materials, **2018.** *89,* 52-66.